PCCP

PAPER

View Article Online
View Journal | View Issue

Cite this: Phys. Chem. Chem. Phys., 2019, 21, 17792

Received 14th July 2019,
Accepted 25th July 2019

DOI: 10.1039/c9cp03947c

rsc.li/pccp

Surface crystallization of ionic liquid crystals†

Mónia A. R. Martins,[abc] Pedro J. Carvalho,[a] Douglas Alves,[d] Claudio Dariva,[d] Mariana C. Costa,[e] Rute A. S. Ferreira,[f] Paulo S. André,[g] Pedro Morgado,[h] Simão P. Pinho,[bc] Eduardo J. M. Filipe[h] and João A. P. Coutinho*[a]

The evidence for surface crystallization in ionic liquids is scarce. The existing reports seem to be contradictory as for its driving forces, since in the two compounds investigated in the literature, the contribution of coloumbic and van der Waals forces is very different. In this work 1-dodecyl-3-methylimidazolium tetrafluoroborate was studied and its surface crystallization characterized by surface tension, ellipsometry and optical microscopy. The results obtained seem to reconcile previous observations, and it was further shown, using the same techniques, that this phenomenon is prevalent in other ionic liquids. MD simulation results illustrate the different possibilities of organization, providing reasonable models to rationalize the experimental observations.

Introduction

Ionic liquid crystals (ILCs) combine the ionic character of ionic liquids (ILs) with the benefits of liquid crystal (LC) anisotropy. They are characterized by long alkyl side chains, relatively low melting points and at least one liquid-crystalline mesophase. Due to their potential applications in diverse fields, this class of compounds has been extensively investigated.[1,2]

Applications involving ILCs rely on their interfaces, detailed knowledge and understanding of their surfaces thus being important. While the surface and surface properties of ionic liquids have been extensively studied,[3–6] studies on the surface of ILCs are scarce. The near-surface structure of $[C_{18}C_1im][FAP]$ was investigated through X-ray absorption spectroscopy and resonant soft X-ray reflectivity, by Mezger *et al.*,[7] revealing depth-decaying near-surface layering. The authors did not claim however, that the observed surface ordering was akin to a LC. Yet, later Mezger and co-workers[8] studied $[C_{22}C_1im][NTf_2]$ reporting a metastable ILC, identifying for the first time a surface induced smectic layer at temperatures up to 90 K above the melting point. Close to the bulk melting point, the thickness of the ordered layer was 30 nm. On an extensive study of the surface of the $[C_nC_1im][NTf_2]$ series[7] the authors reported that $[C_{22}C_1im][NTf_2]$ was the first IL of the series to exhibit this behavior.

Similar to the surface freezing observed in alkanes, where an ordered monolayer is formed on the surface of a disordered bulk liquid,[9] in liquid crystals a smectic phase is formed at the surface of a nematic or isotropic liquid bulk at temperatures above the bulk transition temperature. Several surface phenomena like surface-induced order or surface ordering, wetting, and anchoring are characteristic of thermotropic liquid crystals, as extensively studied by Lucht and co-workers.[10–15] The authors showed that the structure of the LC free surface can be very different from the bulk. The differences resulting from the molecular interactions at or close to the surface, induce the formation of a higher-ordered surface phase, different from that of the bulk.[16,17]

Only two works have so far been reported on the surface crystallization of ionic liquids of a widely different nature. Jeon *et al.*[18] studied a short-chain Coulomb-dominated IL ($[C_4C_1im][PF_6]$) observing the formation of four-layered, rectangularly packed, crystalline domains covering 5–15% of the surface. Pontoni *et al.*,[19] using a long-chain vdW-dominated IL ($[C_{20}C_1im][NTf_2]$) observed a hexagonal crystalline monolayer covering the whole surface. As argued by the authors, the dense packing of alkyl chains, vertically aligned normal to the surface, requires the presence of long-chain impurities.

This work aims at studying the surface of ILCs at temperatures from the melting point to above the clearing point. For

[a] CICECO, Department of Chemistry, Univ. Aveiro, Portugal. E-mail: jcoutinho@ua.pt
[b] Associate Laboratory LSRE-LCM, Polytechnic Institute of Bragança, Portugal
[c] CIMO – Mountain Research Center, Polytechnic Institute of Bragança, Portugal
[d] Institute of Research and Technology, UNIT, Brazil
[e] School of Chemical Engineering, Univ. of Campinas, Brazil
[f] CICECO, Department of Physics, Univ. Aveiro, Portugal
[g] IT and DECE, IST – Univ. of Lisbon, Portugal
[h] Centro de Química Estrutural, IST – Univ. of Lisbon, Portugal

† Electronic supplementary information (ESI) available: $[C_{12}C_1im][BF_4]$ DSC thermograms; experimental values of densities, viscosities and refractive indexes; thermal expansion coefficients and energy barrier calculations; experimental ellipsometric spectra. See DOI: 10.1039/c9cp03947c

this purpose, ILC 1-dodecyl-3-methylimidazolium tetrafluoroborate ($[C_{12}C_1im][BF_4]$) was chosen as a model compound due to its relatively low melting and clearing temperatures, and its large and stable mesophase region.[3,20–22] Its choice relied also on the intermediate nature of the interactions present, when compared with the ILs previously studied *via* surface freezing, in terms of the van der Waals interactions due to its medium size alkyl chain length, yet with strong coulombic interactions resulting from the $[BF_4]^-$ anion. This ILC was shown to be an exceptional medium for the selective synthesis of monoacylglycerides[23] and a promising nuclear magnetic resonance (NMR) alignment medium.[24]

Experimental

Chemicals

The ionic liquid crystal 1-dodecyl-3-methylimidazolium tetrafluoroborate ($[C_{12}C_1im][BF_4]$, CAS 244193-56-4, M = 338.24 g mol^{-1}) was purchased from Iolitec with a purity of >98% (according to the supplier). Prior to each measurement and in order to reduce impurities, like water and volatile compounds, individual samples of $[C_{12}C_1im][BF_4]$ were dried under vacuum (0.1 Pa), moderate temperature (313.15 K) and constant stirring, for a minimum period of 48 h. The water content of the dried samples was determined using a Metrohm 831 Karl Fischer coulometer, with the analyte Hydranal® – Coulomat AG obtained from Riedel-de Haën, and was found to be below 100 ppm for all samples. The chemical structure of this compound is present in Fig. 1. In addition, the following compounds were also used: 1-methyl-3-tetradecylimidazolium tetrafluoroborate ($[C_{14}C_1im][BF_4]$, CAS 244193-61-1, M = 266.28 g mol^{-1}, Iolitec, 98%), 1-dodecyl-3-methylimidazolium chloride ($[C_{12}C_1im]Cl$, CAS 114569-84-5, M = 286.89 g mol^{-1}, Iolitec, >98%), 1-methyl-3-tetradecylimidazolium chloride ($[C_{14}C_1im]Cl$, CAS 171058-21-2, M = 314.94 g mol^{-1}, Iolitec, 98%), 1-methyl-3-tetradecylimidazolium bromide ($[C_{14}C_1im]Br$, CAS 471907-87-6, M = 359.39 g mol^{-1}) and dimethylditetradecylammonium chloride ($[N_{111414}]Cl$, CAS 10108-91-5, M = 474.29 g mol^{-1}). $[C_{14}C_1im]Br$ and $[N_{111414}]Cl$ were synthesized in our laboratory.[25]

Methods

Differential scanning calorimetry (DSC)

The thermal events of the pure ILC were determined using a Hitachi DSC7000X model working at atmospheric pressure and coupled to a liquid nitrogen cooling system. Samples of approximately 5 mg, tightly sealed in aluminum pans, were submitted to a heating–cooling–heating regime at least 3 times. The heating and cooling rates were 1 K min^{-1} and 2 K min^{-1}, respectively. The melting temperatures were taken as the peak temperatures. The equipment was previously calibrated with anthracene, benzoic acid, caffeine, decane, diphenylacetic acid, heptane, indium, lead, naphthalene, 4-nitrotoluene, potassium nitrate, tin, water and zinc; all with weight fraction purities higher than 99%.

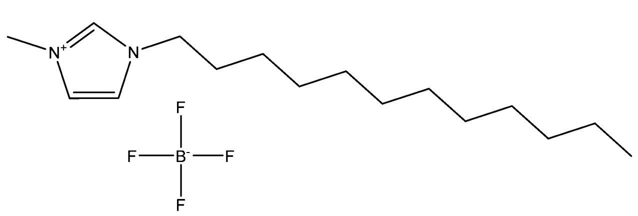

Fig. 1 Structure of 1-dodecyl-3-methylimidazolium tetrafluoroborate.

Density and viscosity

Density measurements of the pure ILC $[C_{12}C_1im][BF_4]$ were carried out at atmospheric pressure and in the 303.16 to 363.14 K temperature range, using an Anton Paar GmbH 4500 vibrating-tube densimeter (Graz, Austria). Two integrated Pt 100 platinum thermometers provided good precision of the internal temperature control (±0.01 K) and the densimeter includes an automatic correction for the viscosity of the sample. The overall uncertainty of the measurements was estimated to be better than 5×10^{-5} g cm^{-3}. Viscosities were carried out using an automated SVM 3000 Anton Paar rotational Stabinger viscometer–densimeter (temperature uncertainty: 0.02 K; dynamic viscosity relative uncertainty: 0.35%), working at atmospheric pressure. Measurements were performed in the temperature range from 319.75 to 373.15 K.

Interfacial tension

Three different setups were used: the interfacial tension setup: a Dataphysics contact angle system OCA-20 was used to determine the surface tension of the ILC $[C_{12}C_1im][BF_4]$ through the analysis of the shape of a pendant drop. A Hamilton DS 500/GT syringe connected with a Teflon coated needle was used to form the drops with volumes of (9 ± 1) μL. The needle was placed inside an aluminium air chamber able to maintain the temperature control within 0.1 K. The temperature was attained by circulating water in a double-jacketed aluminum cell by means of a Julabo F-25 water bath. This temperature was measured with a Pt100, placed at a distance of approximately 1 cm from the liquid drop. After temperature stabilization, drops were formed and allowed to thermally stabilize for 30 minutes prior to the surface tension determination. To ensure a dry environment, silica gel was placed inside the closed aluminum chamber and the cell was kept sealed during the measurements. For each temperature, at least 2 drops were formed and for each drop, an average of 200 images was captured. The analysis of the drop shape was performed using the software module SCA 20 where the gravitational acceleration (g = 9.8018 m s^2) and latitude (lat = 40°) were used according to the location of the assay. The density values required for the calculation of the surface tensions were measured in this work. Furthermore, details on the equipment and its validity to measure surface tensions of ILs can be found in previous publications.[26,27] The high temperature interfacial tension setup: surface tensions of $[C_{12}C_1im]Cl$ and $[C_{14}C_1im][BF_4]$ were determined using the pendant drop method in the 378 to 410 K temperature range. Drops (≈7 μL) were produced using a micrometric syringe (Gilmont Instruments) connected to a Teflon tube, which was introduced inside a Ramé-Hart chamber (model 100-07-00). At high temperatures, the micrometric syringe was heated using a heating tape. The liquid drops were held between the parallel faces of an aluminum block kept inside the chamber at a constant temperature (±0.05 K) using a PID controller. The temperature of the liquid drop was additionally monitored using a differential copper constantan thermocouple. The ambient chamber was dried using silica gel and the chamber flushed using dry nitrogen. A camera (jAi CV-A50) coupled to a Wild M3Z microscope was used to analyze the shape of the pendant drops and their analysis performed using the ADSA-P software (Axisymmetric Drop Shape Analysis, Applied Surface Thermodynamics Research Associates, Toronto, Canada). The estimated overall uncertainty in the temperature measurements is 0.5 K. At least 5 drops were formed at each temperature and 5 images were captured for each drop. Additional details can be found elsewhere.[28,29] Interfacial elasticity setup: measurements on the interfacial tension were carried out on a pendant drop tensiometer (Teclis Tracker, IT Concept) using dynamic oscillatory tests at different temperatures (316–326 K). The ILC was placed in a vertical syringe and drops were formed and aged for 5 minutes, creating an ILC–air interface. Sinusoidal deformations around the interfacial area with oscillation frequencies of 0.05, 0.1, and 0.2 Hz were then performed. No frequency influence was observed in the results. The first few drops formed were discarded and the experiments were performed in triplicate. The profile of each drop formed was scanned by a CCD camera and treated by a personal computer. The equipment software calculates the dynamic interfacial tension by fitting the drop profile with the Young–Laplace equation. The total viscoelastic modulus – and its elastic and viscous components – of the film were derived from the dilatational rheological experiments. Due to the high viscosity of the ILC sample, the drop creation and the dynamic tests were performed with rigid control of the drop area and volume and oscillation amplitude, aiming at a greater reproducibility of the results. In addition, the best volume values and drop area which would produce results with lower noise in the determined properties were evaluated.

The total dilatation modulus (or elasticity) gives values of resistance to the creation of an interfacial tension gradient. The interfacial dilatational module, ε, is defined as the increase of the interfacial tension per unit of increment of surface area (A), being mathematically defined as[30]

$$\varepsilon = \frac{\mathrm{d}\gamma}{\mathrm{d}\ln A} \tag{1}$$

where γ is the interfacial tension (mN m^{-1}) and A is the interfacial surface (mm^2). When an oscillatory deformation is applied, the elasticity presents an imaginary component (ε'') and a real component (ε') defined by an oscillatory area, where the first term is equal to the elastic contribution and the second is proportional to the viscous contribution:

$$\varepsilon = \varepsilon' + \varepsilon'' i \tag{2}$$

Further details on experimental conditions can be found elsewhere.[31,32]

Light-polarized optical microscopy

The melting profile of the ionic liquid crystal $[C_{12}C_1im][BF_4]$ was evaluated using an Olympus BX51 light polarized microscope (Olympus Co., Tokyo, Japan) coupled to a Linkam LTS120 temperature-controlled peltier system (Linkam Scientific Instruments, Ltd, Tadworth, U.K.) with a precision of ±0.05 K. The optical textures of $[C_{14}C_1im][BF_4]$, $[C_{12}C_1im]Cl$, $[C_{14}C_1im]Cl$, $[C_{14}C_1im]Br$ and $[N_{111414}]Cl$ were captured using an optical microscope Leica DM 2700 M with a temperature controller Linkam LTS 420. Samples of around 1 mg were placed in a conclave glass slide, covered with a lamella and sealed with thermal glue in order to avoid the adsorption of water. Different heating and cooling rates were applied, and are described and analyzed in the Results section.

Ellipsometry

The spectroscopic ellipsometry measurements were carried out using an AutoSE ellipsometer (HORIBA Scientific) with a total of 250 points in the wavelength interval of 450–850 nm, an incidence angle (θ_0) of 69.8° and a signal to noise ratio of 30. A measurement spot area of 250 × 250 μm^2 was used. Three measurements were performed for each temperature. The temperature of the sample was controlled by using a Peltier system. The refractive index values were calculated assuming a three-layered structure model consisting of one layer for the $[C_{12}C_1im][BF_4]$ ILC bulk material, a surface layer, and a layer of air as an ambient medium. The data were minimized using the Simplex algorithm, and the dispersion curves were determined using the Cauchy absorbent model, given by:

$$n(\lambda) = A + \frac{B}{\lambda^2} + \frac{C}{\lambda^4} \tag{3}$$

where n is the refractive index, λ is the wavelength (nm), and A, B and C are constants.

Refractive Index

Refractive index (n_D) measurements were performed at 589.3 nm using an automated Abbemat 500 Anton Paar refractometer (maximum temperature deviation: ±0.01 K; maximum refractive index uncertainty: 2 × 10^{-5}). Measurements were carried out in the temperature range from (308 to 322) K and at atmospheric pressure. The device uses reflected light to measure the refractive index where the sample on the top of the measuring prism is irradiated from different angles by using a light-emitting diode.

Results and discussion

On heating, $[C_{12}C_1im][BF_4]$ first melts to a viscous smectic A mesophase[3,20–22] which then turns into an isotropic liquid. The solid–liquid crystal–isotropic liquid phase transitions (hereby called melting and clearing points, respectively) of the tetrafluoroborate-based ILC were measured by DSC and these results, presented in Table 1, are in good agreement with the literature.[20–22] The clearing point was further confirmed *via* polarizing optical microscopy (POM). At times, this compound

Table 1 Phase transition temperatures and enthalpies of $[C_{12}C_1im][BF_4]$ and comparison with literature data

	Solid → liquid crystal		Liquid crystal → liquid	
	Heating	Cooling	Heating	Cooling
T/K	302.94 ± 1.87	286.15 ± 1.39	320.20 ± 0.27	319.67 ± 0.16
	299.55[a]	280.55[a]	311.65[a]	310.15[a]
	285.37[b]	287.33[b]	323.17[b]	323.95[b]
	305.75[c]	283.25[c]	322.45[c]	319.85[c]
ΔH_{fus}/kJ mol^{-1}	27.05 ± 2.81	26.26 ± 3.40	0.30 ± 0.03	0.31 ± 0.03
	29.6[a]	23.7[a]	0.3[a]	0.2[a]
	26.1[b]	18.1[b]	0.3[b]	0.2[b]
	26.2[c]	26.3[c]	0.3[c]	0.3[c]

[a] Holbrey and Seddon, 1999.[20] [b] Larionova *et al.*, 2009.[21] [c] Zhang *et al.*, 2012.[22]

displays a reversible crystal–crystal transition at T_{ss} = 300.62 ± 0.34 K, in the second and/or third heating cycle (see Fig. S1 of the ESI†); a similar thermotropic polymorphic behavior was already reported for 1-alkyl-3-methylimidazolium tetrachloropalladate(II) salts.[33]

To fully characterize the $[C_{12}C_1im][BF_4]$ bulk properties, the density, viscosity, and refraction index were measured and are reported in the ESI.† Densities and viscosities of pure $[C_{12}C_1im][BF_4]$ were measured at several temperatures and at atmospheric pressure, and are listed in Table S1 and presented in Fig. S2 and S3 (ESI†). The experimental refractive indices for pure $[C_{12}C_1im][BF_4]$ are listed in Table S2 (ESI†). To the best of our knowledge, there are no data available for comparison in the open literature. The densities and refractive indexes display clear transitions at around 320 K which are in agreement with the clearing point measured. Due to the density, there is a clear variation on the isobaric thermal expansion coefficient (Fig. S2, ESI†) corresponding to a change in behavior due to an increase in the disorganization of the liquid phase. The refractive index also presents a sudden decrease as the liquid becomes isotropic. Although the viscosity also presents a significant change around the clearing point it was not possible to measure the viscosity of $[C_{12}C_1im][BF_4]$ in the liquid crystal phase because it was outside the range of our apparatus.

To study the surface of the $[C_{12}C_1im][BF_4]$ ILC, measurements of the surface tension of the liquid crystal and isotropic liquid were carried out. Due to the high viscosity of the liquid phase, surface tension measurements were only possible above 317 K, as shown in Fig. 2a. The results reveal a clear change of slope at around 322 K. This change of slope was shown to be reversible. Although this behavior was not reported by Law and Watson,[34] upon close inspection of their data for $[C_{12}C_1im][BF_4]$, an inversion of slope seems to be present at the lowest temperatures, although within the experimental uncertainty of the data.

Information on the surface excess entropy can be taken from the temperature slope of the surface tension[9,35] using $d\gamma/dT = -(S_s - S_b)$, where S_s and S_b are the entropies for the surface and the bulk, respectively. A negative temperature slope indicates that the molecules on the surface are less constrained than those in the bulk ($S_s > S_b$). The ordering of the liquid surface results in a surface entropy reduction and thus $S_s < S_b$ and $d\gamma/dT > 0$. A change in slope for the surface tension is thus a

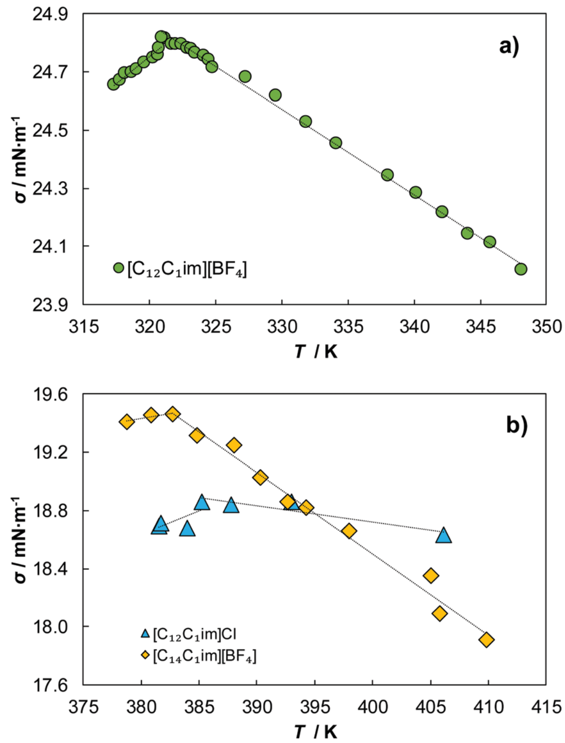

Fig. 2 Temperature dependence of the surface tension, σ, of $[C_{12}C_1im][BF_4]$, $[C_{14}C_1im][BF_4]$ and $[C_{12}C_1im]Cl$, measured using two different setups (description available in the ESI†). The lines are guides for the eyes.

strong indicator of an ordering transition at the surface. This behavior, observed here for $[C_{12}C_1im][BF_4]$, and previously reported for the *n*-alkanes, liquid metal SDS/water solutions,[9,35] and in liquid crystals around the nematic to isotropic transition,[36] is a clear indication of the formation of a liquid crystalline[10–15,36] or solid layer[4,7,9,35] at the surface of the isotropic liquid. First order transitions are characterized by small negative slopes for the liquid surface and large positive ones on the order crystalline surface as observed for alkanes.[9] This is translated by the entropy change upon formation of the surface layer, $\Delta S_s = d\gamma/dT_{surface} - d\gamma/dT_{liquid}$, calculated as the difference between the slope of the surface tension below and above the layer formation temperature. For $[C_{12}C_1im][BF_4]$, ΔS_s has a value of 0.066 mN m^{-1} K^{-1}, considerably lower than the values of ΔS_s presented for *n*-alkanes (for example: for hexadecane $n = 16$, and $\Delta S_s = 0.896$ mN m^{-1} K^{-1}).[9] In addition, it is possible to calculate the entropy change in the bulk liquid-rotator transition or bulk freezing, $\Delta S_b = \mathrm{d}\gamma/\mathrm{d}T_{\mathrm{rotator}} - \mathrm{d}\gamma/\mathrm{d}T_{\mathrm{liquid}}$, that gives information about the similarity between the ordered monolayer and that of the bulk rotator phase.[9] $\mathrm{d}\gamma/\mathrm{d}T_{\mathrm{rotator}}$ can be approximated from latent heat measurements[35] using the melting properties presented in Table 1. Thus, by taking an average area per molecule of 45 Å^2,[37] one can calculate $\Delta S_b = 0.359$ mN m^{-1} K^{-1}. As expected, the entropy change upon bulk freezing is higher than the entropy change upon surface freezing, given the more organized nature of the anisotropic liquid phase on top of which the surface crystal develops.

Information on the surface excess entropy can be taken from the temperature slope of the surface tension[9,35] using $\mathrm{d}\gamma/\mathrm{d}T = -(S_s - S_b)$, where S_s and S_b are the entropies for the surface and the bulk, respectively. A negative temperature slope indicates that the molecules on the surface are less constrained than those in the bulk ($S_s > S_b$). The ordering of the liquid surface results in a surface entropy reduction and thus $S_s < S_b$ and $\mathrm{d}\gamma/\mathrm{d}T > 0$. A slope change in the surface tension is thus a strong indicator of an ordering transition at the surface. This behavior, observed here for $[C_{12}C_1im][BF_4]$, and previously reported for the *n*-alkanes, liquid metal SDS/water solutions,[9,35] and in liquid crystals around the nematic to isotropic transition,[36] is a clear indication of the formation of a liquid crystalline[10–15,36] or solid layer[4,7,9,35] at the surface of the isotropic liquid. First order transitions are characterized by small negative slopes in the liquid surface and large positive ones in the order crystalline surface as observed for alkanes.[9] This is translated by the entropy change upon formation of the surface layer, $\Delta S_s = \mathrm{d}\gamma/\mathrm{d}T_{\mathrm{surface}} - \mathrm{d}\gamma/\mathrm{d}T_{\mathrm{liquid}}$, calculated as the difference between the slope of the surface tension below and above the layer formation temperature. For $[C_{12}C_1im][BF_4]$, ΔS_s has a value of 0.066 mN m^{-1} K^{-1}, considerably lower than the values of ΔS_s presented for *n*-alkanes (for example: for hexadecane $n = 16$, $\Delta S_s = 0.896$ mN m^{-1} K^{-1}).[9] In addition, it is possible to calculate the entropy change in the bulk liquid-rotator transition or bulk freezing, $\Delta S_b = \mathrm{d}\gamma/\mathrm{d}T_{\mathrm{rotator}} - \mathrm{d}\gamma/\mathrm{d}T_{\mathrm{liquid}}$, which gives information about the similarity between the ordered monolayer and that of the bulk rotator phase.[9] $\mathrm{d}\gamma/\mathrm{d}T_{\mathrm{rotator}}$ can be approximated from latent heat measurements[35] using the melting properties presented in Table 1. Thus, by taking an average area per molecule of 45 Å^2,[37] one can calculate $\Delta S_b = 0.359$ mN m^{-1} K^{-1}. As expected, the entropy change upon bulk freezing is higher than the entropy change upon surface freezing, given the more organized nature of the anisotropic liquid phase on top of which the surface crystal develops.

Having identified the existence of a surface ordering phenomenon at the surface of the smectic $[C_{12}C_1im][BF_4]$ ILC, and two other ILCs, and aiming to further probe the interfacial reorganization, the interfacial elasticity (ε), and its elastic (ε'), and viscous (ε'') modulii were evaluated for $[C_{12}C_1im][BF_4]$ at different temperatures, as depicted in Fig. 3. Above 323 K the values of ε are close to zero, suggesting no interfacial reorganization during the oscillations and thus, that the system presents the behavior of an isotropic liquid.[38] At lower temperatures an increase in the total interfacial elasticity is observed, indicating that reorganization takes place at the interface. Furthermore, a clear dependence of ε on temperature suggests a continuous increase in the interfacial activity, with the behavior depicted in Fig. 3b indicating that this interface behavior is almost purely elastic. Despite the high bulk viscosity of the compound at these temperatures, the viscous and elastic modulii are related to the interface features. While the viscous modulus associated to the liquid-like structural characteristics of the interface remains constant and close to zero, the essentially elastic behavior of the surface denotes a solid-like structure, showing that we are in the presence of a surface freezing phenomenon similar to that observed by Pontoni *et al.*[19]

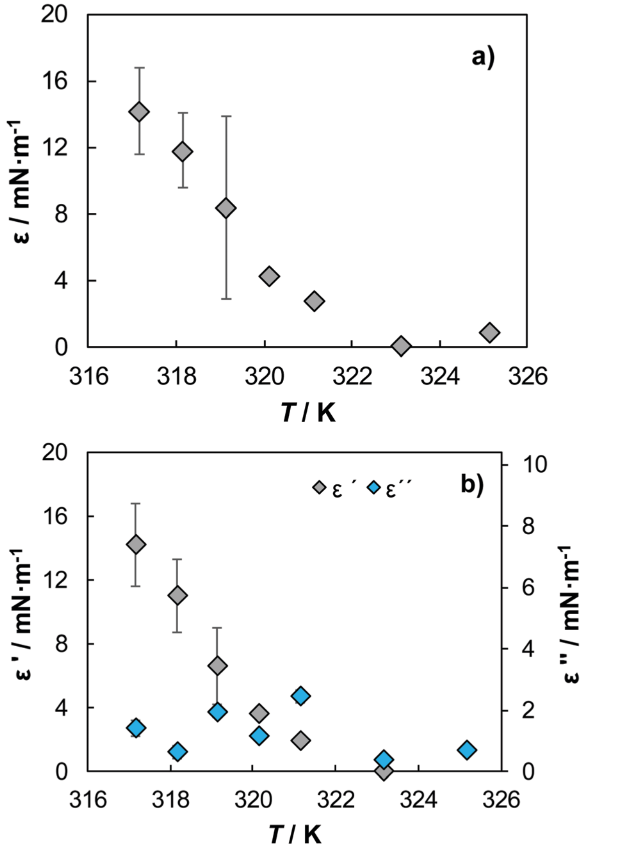

Fig. 3 Interfacial elasticity (ε), and its elastic (ε') and viscous (ε'') components as a function of temperature and at a frequency of 0.05 Hz.

To further investigate the surface freezing, polarized optical microscopy observations of the phase transitions were carried out, revealing some very interesting textures at a length scale accessible to direct observation, as shown in Fig. 4. On heating it is possible to see the disappearance of the liquid crystals together with some specific structures with a diameter of around 5 μm. These structures decrease in number and size with increasing temperature, but persist after the clarification of the bulk liquid crystal. The same phenomenon is observed during cooling, where an initial appearance of the micrometric structure and its reorganization at the surface of the isotropic

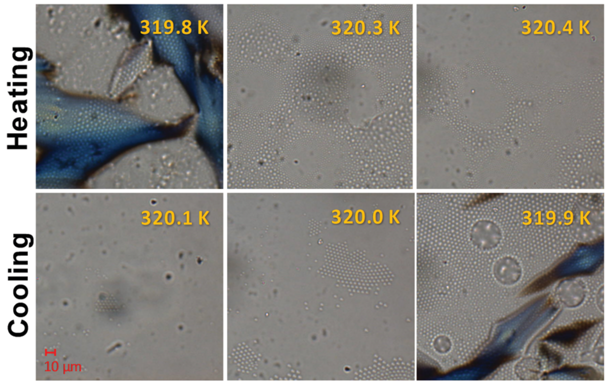

Fig. 4 Optical textures of $[C_{12}C_1im][BF_4]$ at different temperatures (heating and cooling rates of 0.1 K min^{-1}).

liquid is observed, followed by the appearance of the bulk liquid crystals (a video is available in the ESI†). The same behavior was also observed for two other ILCs, namely $[C_{14}C_1im][BF_4]$ and $[C_{12}C_1im]Cl$, for which the surface tension is reported here, along with the surface tension reported for $[C_{14}C_1im]Cl$, $[C_{14}C_1im]Br$ and $[N_{111414}]Cl$ as shown in Fig. 5.

Although a more detailed characterization of these structures was not possible with the experimental techniques available, our interpretation of these observations is based on the experiments of Jeon *et al.*[18] in the presence of crystalline domains at the surface of an isotropic ionic liquid. Pontoni *et al.*[19] distinguish the surface crystallization with a full surface coverage for $[C_{20}C_1im][NTf_2]$ with vdW-dominated interactions, from the crystalline domains observed on Coulomb-dominated $[C_4C_1im][PF_6]$. The intermediate chain length of the ILs studied here, combined with the strongly charged anions Cl^- and $[BF_4]^-$, induce a behavior that bridges the two types of surface freezing on ILs observed previously: from the crystalline domains and partial coverage on top of an isotropic liquid at high temperatures above the clearing point, to a full coverage on top of a liquid crystalline phase at temperatures below the clearing point.

Aiming to further characterize the ordered surface of $[C_{12}C_1im][BF_4]$ and to support the interpretation of the results reported above, the $[C_{12}C_1im][BF_4]$ refractive index, dispersion curves and thickness were measured *via* spectroscopic ellipsometry as a function of temperature (see the ESI† for detailed results in Fig. S4 and S5). As can be seen in Fig. 6, there is a discontinuous transition in the refractive index measured using both refractometry and ellipsometry techniques. This behavior confirms the appearance of an ordered surface. In addition, it was possible to measure the thickness of the surface layer that continuously decreases with increasing temperature. The layer disappears around 323 K, somewhat above the clarification point in agreement with the transitions observed with the other techniques used here. One slope change can be seen at the liquid crystal–liquid phase transition. This behavior previously observed before for LCs was described as a wetting phenomenon.[11]

In order to obtain molecular level insight into the studied system, the surface of bulk phases of the $[C_{12}C_1im][BF_4]$ IL, the isotropic liquid and the smectic liquid crystal at different temperatures, was also studied by atomistic molecular dynamic simulations. As will be shown, the simulation results illustrate different possibilities of surface organization, thus contributing to the interpretation of the experimental observations and an overall understanding of the phenomenon.

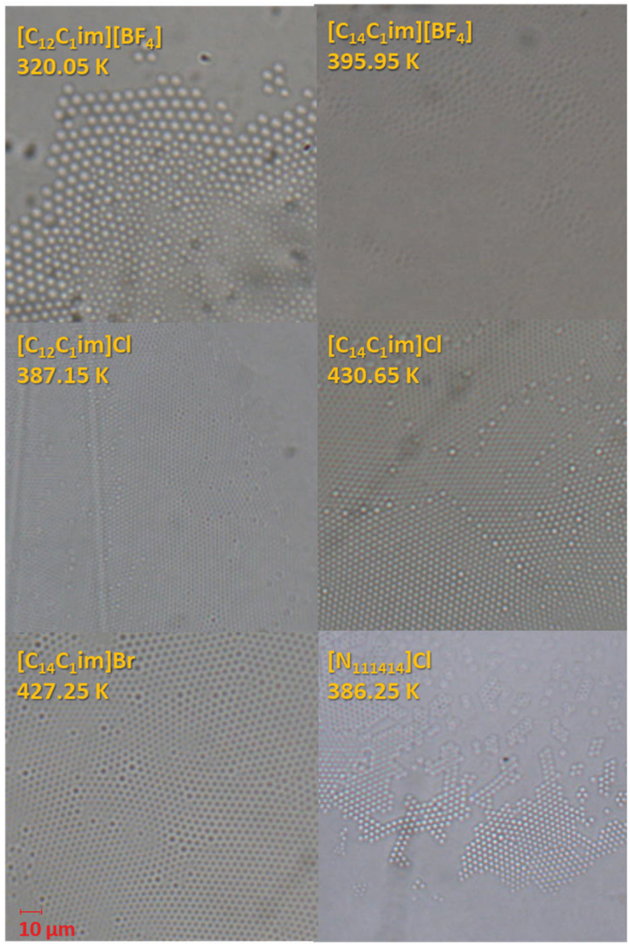

Fig. 5 Optical textures of $[C_{14}C_1im][BF_4]$, $[C_{12}C_1im]Cl$, $[C_{14}C_1im]Cl$, $[C_{14}C_1im]Br$ and $[N_{111414}]Cl$ at different temperatures.

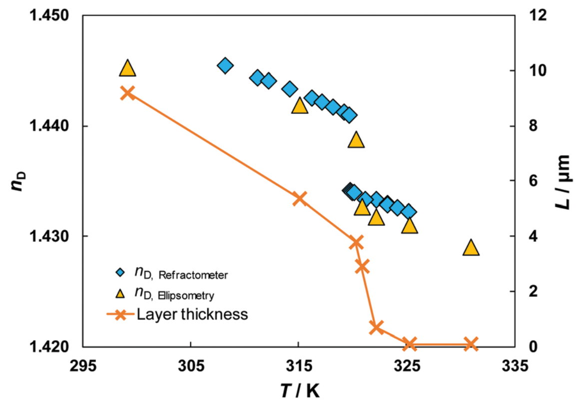

Fig. 6 Experimental refractive index, n_D, at 589 nm of pure $[C_{12}C_1im][BF_4]$ and the thickness, L, of the liquid crystal layer as a function of temperature.

The CL&P force field was used to model the ionic liquid.[39] The simulation of the isotropic liquid started from a random low density configuration of 1000 ion pairs and was equilibrated in the *NVT* ensemble in an elongated box with a volume corresponding to a state of liquid–vapour coexistence. The liquid crystalline phase was simulated following the approach proposed and validated by Bruce *et al.*[40] and extending the simulation box in the direction perpendicular to the smectic layers, in order to explicitly obtain two liquid–vacuum interfaces. The liquid crystalline structure was then frozen by gradually lowering the temperature until a structure very close to the crystalline solid was recovered. The full simulation details are presented in the ESI.†

The interfacial structures were analysed by obtaining the atomic density profiles, in the direction normal to the liquid–vacuum interface, from the simulation trajectories. The density profiles for the anion, the charged part of the cation and the terminal group of the cation side chain are shown in Fig. 7, together with simulation snapshots of the corresponding structures.

As seen in Fig. 7 (middle), the liquid crystalline smectic phase displays a well-defined layered structure formed by distinct ionic bilayers. Within each layer, the anions and the charged part of the cations alternate in a plane, forming a checkerboard distribution. The ionic bilayers alternate forming layers of dense, interdigitated, alkyl side-chains.

On cooling, as could be expected, the system clearly becomes denser and more organized (Fig. 7 (top)). The profile peaks become slightly narrower, reflecting the lower mobility of the particles and higher density. The interdigitated alkyl side-chains adopt a tilted conformation and distinct packing planes become visible. The structure is believed to be very close to a crystalline solid, although the profile peaks are slightly broader than those of a typical solid.

In the isotropic liquid phase (Fig. 7 (bottom)), the ionic bilayered fine structure of the liquid crystal is completely lost. Single peaks now appear in the density profiles of both the charge groups and alkyl side-chains, revealing a fully liquid-like organization. The alkyl side-chains lost the previous recognisable interdigitated structure.

Regarding the surfaces, the simulation results are again able to illustrate the different possibilities of organization, providing reasonable models to rationalize the experimental observations.

The isotropic liquid surface shows a layered structure that decays with the distance from the interface (and also with temperature). It is often argued[7] that this "conventional" surface layering, which increases at lower temperatures, gradually propagates to the bulk of the liquid. At the clearing temperature the whole system will be liquid-crystalline. It is also apparent that the alkyl side-chains, as expected preferentially oriented towards the vacuum, are relatively disorganized. This results from the low density of side-chains at the interface that precludes an effective close-packing of the chains and an efficient coverage of the charged moieties.

The surface of the liquid crystalline mesophase is clearly more organized than that of the isotropic liquid and is compatible with a liquid crystal surface phase.[19] This already displays

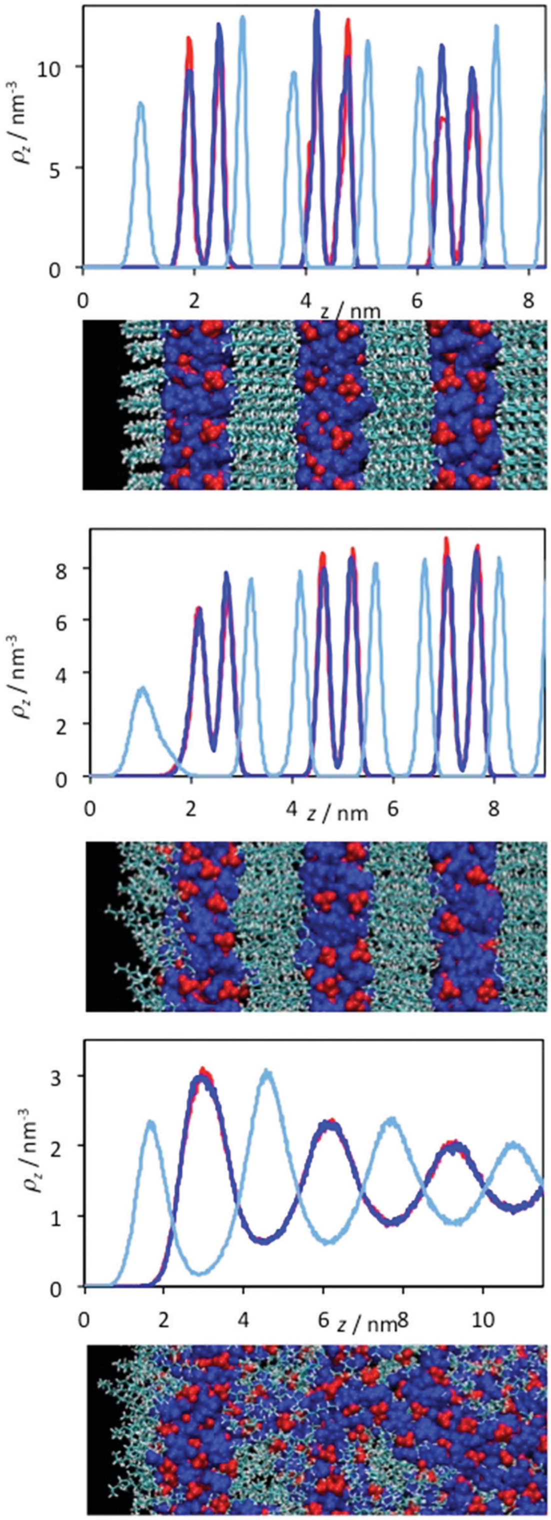

Fig. 7 Simulation snapshots and surface normal atomic density profiles for the solid (top), liquid crystal (middle) and isotropic liquid (bottom) surfaces. Profiles: dark blue = charged part of cation (C atom between the N atoms), red = anion (B atom), light blue = terminal methyl carbon of the C12 chain. Snapshots: charged parts are represented by blue (cation) and red (anion) van der Waals spheres; the C12 side chain is represented by light blue and white wireframe.

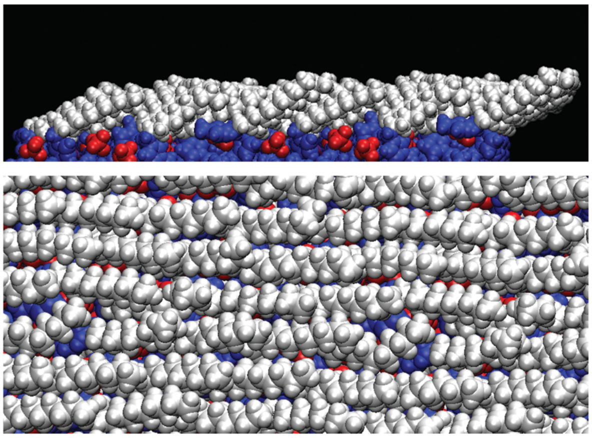

Fig. 8 Simulation snapshots of the surface of the solid: (top), side view; (bottom) top view. Colour scheme as shown in Fig. 7.

the characteristic checkerboard plane configuration of the ionic parts. However, the alkyl side chains are still relatively disorganized.

On cooling, it is clear from Fig. 7 (bottom) and 8 that a highly organized structure is formed at the surface. The alkyl chains now adopted a highly tilted configuration that simultaneously allows close packing of the chains and an efficient coverage of the surface. This structure is compatible with a solid crystalline surface and in our opinion is a good model for the solid-like, highly organized surface evidenced by the experimental results. The simulation results also indicate that the formation of a stable organized solid-like structure at the surface of an ILC does not require the presence of an impurity particle to increase the density of chains (Fig. 8).

Conclusions

This work studied the surface of $[C_{12}C_1im][BF_4]$ at temperatures from the melting point to above the clearing point. This compound was chosen due to its low melting and clearing temperatures and large and stable mesophase. The nature of the interactions present when compared with the ILs previously reported to show surface freezing allows it to link the two extreme types of surface behavior reported: formation of crystal domains in coulombic dominated ILs or full coverage for long chain, van der Waals dominated ILs. The experimental techniques used here support the presence of crystalline domains at the surface of the isotropic liquid, fully covering the surface of the liquid crystalline mesophase. The solid nature of this layer, demonstrated here by the elastic behavior revealed by the surface rheology, is in agreement with the results obtained by using the X-ray method by Pontoni *et al.*[9] Surface tension measurements and optical microscopy suggest that this behaviour is a prevalent phenomenon on this type of compound that would deserve further investigation and characterization. MD simulation results illustrate the different possibilities of organization, providing reasonable models to rationalize the experimental observations.

Conflicts of interest

There are no conflicts to declare.

Acknowledgements

This work was developed with the scope of the project CICECO – Aveiro Institute of Materials, UID/CTM/50011/2019, Associate Laboratory LSRE-LCM, UID/EQU/50020/2019, and of Instituto de Telecomunicações/IT (UID/EEA/50008/2013) – funded by national funds through FCT/MCTES (PIDDAC). M. A. R. M. acknowledges financial support from NORTE-01-0145-FEDER-000006 – funded by NORTE2020 through PT2020 and ERDF, and P. J. C. acknowledges the FCT for the contract IF/00758/2015. A. R. Bastos from UA is acknowledged for help in the ellipsometry measurements. M. C. C. aknowledges FAPESP (2012/05027-1) and CNPq (310272/2017-3) for financial support.

References

1 K. Binnemans, Ionic liquid crystals, *Chem. Rev.*, 2005, **105**, 4148–4204.
2 K. Goossens, K. Lava, C. W. Bielawski and K. Binnemans, Ionic Liquid Crystals: Versatile Materials, *Chem. Rev.*, 2016, **116**, 4643–4807.
3 X. Zhu, H. Li, Z. Wang, C. Yuan, P. Zhu, L. Su, K. Yang, J. Wu, G. Yang and X. Li, Pressure-induced ionic liquid crystal in 1-dodecyl-3-methylimidazolium tetrafluoroborate, *RSC Adv.*, 2017, **7**, 26428–26433.
4 E. Sloutskin, B. M. Ocko, L. Tamam, I. Kuzmenko, T. Gog and M. Deutsch, Surface Layering in Ionic Liquids: An X-ray Reflectivity Study, *J. Am. Chem. Soc.*, 2005, **127**, 18333.
5 K. R. J. Lovelock, I. J. Villar-Garcia, F. Maier, H.-P. Steinrück and P. Licence, Photoelectron Spectroscopy of Ionic Liquid-Based Interfaces, *Chem. Rev.*, 2010, **110**, 5158–5190.
6 S. P. M. Ventura, F. A. E. Silva, M. V. Quental, D. Mondal, M. G. Freire and J. A. P. Coutinho, Ionic-Liquid-Mediated Extraction and Separation Processes for Bioactive Compounds: Past, Present, and Future Trends, *Chem. Rev.*, 2017, **117**, 6984–7052.
7 M. Mezger, B. M. Ocko, H. Reichert and M. Deutsch, Surface layering and melting in an ionic liquid studied by resonant soft X-ray reflectivity, *Proc. Natl. Acad. Sci. U. S. A.*, 2013, **110**, 3733–3737.
8 J. Mars, B. Hou, H. Weiss, H. Li, O. Konovalov, S. Festersen, B. M. Murphy, U. Rütt, M. Bier and M. Mezger, Surface induced smectic order in ionic liquids – an X-ray reflectivity study of $[C_{22}C_1im]^+$ $[NTf_2]-$, *Phys. Chem. Chem. Phys.*, 2017, **19**, 26651–26661.
9 B. M. Ocko, X. Z. Wu, E. B. Sirota, S. K. Sinha, O. Gang and M. Deutsch, Surface freezing in chain molecules: normal alkanes, *Phys. Rev. E: Stat. Phys., Plasmas, Fluids, Relat. Interdiscip. Top.*, 1997, **55**, 3164–3182.
10 R. Lucht, P. Marczuk, C. Bahr and G. H. Findenegg, X-ray reflectivity study of smectic wetting and prewetting at the free surface of isotropic liquid crystals, *Phys. Rev. E: Stat., Nonlinear, Soft Matter Phys.*, 2001, **63**, 041704.

11 R. Lucht and C. Bahr, Wetting Phenomena at the Free Surface of the Isotropic Phase of a Smectic Liquid Crystal, *Phys. Rev. Lett.*, 1997, **78**, 3487–3490.

12 R. Lucht and C. Bahr, Prewetting Critical Point in a Binary Liquid-Crystal System, *Phys. Rev. Lett.*, 1998, **80**, 3783–3786.

13 R. Lucht, C. Bahr, G. Heppke and J. W. Goodby, Variety of wetting behaviors at the free surface of isotropic liquid crystals, *J. Chem. Phys.*, 1998, **108**, 3716–3721.

14 R. Lucht, C. Bahr and G. Heppke, Layering Transitions at the Free Surface of a Smectic Liquid Crystal, *J. Phys. Chem. B*, 1998, **102**, 6861–6864.

15 R. Lucht, C. Bahr and G. Heppke, Wetting behavior above the liquid-crystal–isotropic transition in a homologous series, *Phys. Rev. E: Stat. Phys., Plasmas, Fluids, Relat. Interdiscip. Top.*, 2000, **62**, 2324–2333.

16 W. H. De Jeu, B. I. Ostrovskii and A. N. Shalaginov, Structure and fluctuations of smectic membranes, *Rev. Mod. Phys.*, 2003, **75**, 181–235.

17 C. Y. Matuo, A. Bourdon, A. Bee and A. M. Figueiredo Neto, Surface-induced ordering in ionic and surfacted magnetic fluids, *Phys. Rev. E: Stat. Phys., Plasmas, Fluids, Relat. Interdiscip. Top.*, 1997, **56**, R1310–R1313.

18 Y. Jeon, D. Vaknin, W. Bu, J. Sung, Y. Ouchi, W. Sung and D. Kim, Surface Nanocrystallization of an Ionic Liquid, *Phys. Rev. Lett.*, 2012, **108**, 055502.

19 D. Pontoni, J. Haddad, B. M. Murphy, S. Festersen, O. Konovalov, B. M. Ocko and M. Deutsch, Surface Phases and Surface Freezing in an Ionic Liquid, *J. Phys. Chem. C*, 2019, **123**, 3058–3066.

20 J. D. Holbrey and K. R. Seddon, The phase behaviour of 1-alkyl-3-methylimidazolium tetrafluoroborates; ionic liquids and ionic liquid crystals, *J. Chem. Soc., Dalton Trans.*, 1999, **0**, 2133–2140.

21 J. Larionova, Y. Guari, C. Blanc, P. Dieudonne, A. Tokarev and C. Guérin, Toward Organization of Cyano-Bridged Coordination Polymer Nanoparticles within an Ionic Liquid Crystal, *Langmuir*, 2009, **25**, 1138–1147.

22 S. Zhang, S. Liu, Y. Zhang and Y. Deng, Photoinduced Isothermal Phase Transition of Ionic Liquid Crystals, *Chem. – Asian J.*, 2012, **7**, 2004–2007.

23 P. Lozano, C. Gomez, S. Nieto, G. Sanchez-Gomez, E. García-Verdugo and S. V. Luis, Highly selective biocatalytic synthesis of monoacylglycerides in sponge-like ionic liquids, *Green Chem.*, 2017, **19**, 390–396.

24 M. E. Di Pietro, G. Celebre and G. De Luca, Doped ionic liquid crystals as effective weakly alignment media for polar solutes, *J. Magn. Reson.*, 2016, **267**, 63–67.

25 T. E. Sintra, M. Vilas, M. Martins, S. P. M. Ventura, A. I. M. C. Lobo Ferreira, L. M. N. B. F. Santos, F. J. M. Gonçalves, E. Tojo and J. A. P. Coutinho, Synthesis and Characterization of Surface-Active Ionic Liquids Used in the Disruption of Escherichia Coli Cells, *ChemPhysChem*, 2019, **20**, 727–735.

26 H. F. D. Almeida, P. J. Carvalho, K. A. Kurnia, J. A. Lopes-da-Silva, J. A. P. Coutinho and M. G. Freire, Surface tensions of ionic liquids: non-regular trend along the number of cyano groups, *Fluid Phase Equilib.*, 2016, **409**, 458–465.

27 A. Luís, K. Shimizu, J. M. M. Araújo, P. J. Carvalho, J. A. Lopes-da-Silva, J. N. Canongia Lopes, L. P. N. Rebelo, J. A. P. Coutinho, M. G. Freire and A. B. Pereiro, Influence of Nanosegregation on the Surface Tension of Fluorinated Ionic Liquids, *Langmuir*, 2016, **32**, 6130–6139.

28 M. Tariq, A. P. Serro, J. L. Mata, B. Saramago, J. M. S. S. Esperança, J. N. C. Lopes and L. P. N. Rebelo, High-temperature surface tension and density measurements of 1-alkyl-3-methylimidazolium bistriflamide ionic liquids, *Fluid Phase Equilib.*, 2010, **294**, 131–138.

29 J. Restolho, A. P. Serro, J. L. Mata and B. Saramago, Viscosity and Surface Tension of 1-Ethanol-3-methylimidazolium Tetrafluoroborate and 1-Methyl-3-octylimidazolium Tetrafluoroborate over a Wide Temperature Range, *J. Chem. Eng. Data*, 2009, **54**, 950–955.

30 E. Fuentes-Prado and L. P. Martínez-Padilla, Colloidal stability and dilatational rheology at the air–water interface of peptides derived from thermal-acidic treated wheat gluten, *Food Hydrocolloids*, 2014, **41**, 210–218.

31 D. R. Alves, J. S. A. Carneiro, I. F. Oliveira, F. Façanha, A. F. Santos, C. Dariva, E. Franceschi and M. Fortuny, Influence of the salinity on the interfacial properties of a Brazilian crude oil–brine systems, *Fuel*, 2014, **118**, 21–26.

32 W. J. S. Morais, E. Franceschi, C. Dariva, G. R. Borges, A. F. Santos and C. C. Santana, Dilatational Rheological Properties of Asphaltenes in Oil–Water Interfaces: Langmuir Isotherm and Influence of Time, Concentration, and Heptol Ratios, *Energy Fuels*, 2017, **31**, 10233–10244.

33 C. Hardacre, J. D. Holbrey, P. B. McCormac, S. E. J. McMath, M. Nieuwenhuyzen and K. R. Seddon, Crystal and liquid crystalline polymorphism in 1-alkyl-3-methylimidazolium tetrachloropalladate(II) salts, *J. Mater. Chem.*, 2001, **11**, 346–350.

34 G. Law and P. R. Watson, Surface Tension Measurements of *N*-Alkylimidazolium Ionic Liquids, *Langmuir*, 2001, **17**, 6138–6141.

35 X. Z. Wu, E. B. Sirota, S. K. Sinha, B. M. Ocko and M. Deutsch, Surface crystallization of liquid normal-alkanes, *Phys. Rev. Lett.*, 1993, **70**, 958–961.

36 M. Tintaru, R. Moldovan, T. Beica and S. Frunza, Surface tension of some liquid crystals in the cyanobiphenyl series, *Liq. Cryst.*, 2001, **28**, 793–797.

37 L. Shi and L. Zheng, Aggregation Behavior of Surface Active Imidazolium Ionic Liquids in Ethylammonium Nitrate: Effect of Alkyl Chain Length, Cations, and Counterions, *J. Phys. Chem. B*, 2012, **116**, 2162–2172.

38 R. Miller, R. Wüstneck, J. Krägel and G. Kretzschmar, Dilational and shear rheology of adsorption layers at liquid interfaces, *Colloids Surf., A*, 1996, **111**, 75–118.

39 J. N. Canongia Lopes and A. A. H. Pádua, CL&P: a generic and systematic force field for ionic liquids modeling, *Theor. Chem. Acc.*, 2012, **131**, 1129–1139.

40 D. W. Bruce, Y. Gao, J. N. Canongia Lopes, K. Shimizu and J. M. Slattery, Liquid-Crystalline Ionic Liquids as Ordered Reaction Media for the Diels–Alder Reaction, *Chem. – Eur. J.*, 2016, **22**, 16113–16123.

